TOSCA

TOSCA 101191394

Manufacturing Processes and Digital **To**ols for more **S**ustainable **C**omposite **A**erostructures

Deliverable D4.3: "Sensors for structural health monitoring"

Due date of deliverable: 2026-04-30
Actual submission date: 2026-04-23

Start date of project: 1st January 2025 — Duration: 36 months

Coordinator:
Christian Eitzinger, Profactor

Lead Beneficiary: ITA
Contributions by: GMI, FIDAMC, ADD Composites

Dissemination Level		
PU	Public	X
SEN	Sensitive information	

TOSCA Project is entirely funded by the European Union, under the topic HORIZON-CL5-2024-D5-01-08 of the Horizon Europe Framework Programme (HORIZON). Views and opinions expressed are however those of the author(s) only and do not necessarily reflect those of the European Union or the European Climate, Infrastructure and Environment Executive Agency. Neither the European Union nor the granting authority can be held responsible for them.

Funded by the European Union

History of Changes

Change made	Explanation
2026-04-23 First submission	
2026-08-04 Design change of the front page	EU logo and funding statement was missing
2026-08-04 Minor changes to figure captions	Improved the wording of the captions for Figure 9 and Figure 11

Contents

1. OBJECTIVE

The objective of this deliverable is to describe the sensor network that will be used for structural health monitoring including its integration within the composite and the evaluation of its sensitivity to typical changes of the part over its lifetime.

In TOSCA, a sensor network combining magnetostrictive ribbons and piezoelectric sensors is proposed to monitor two complementary types of damages, failure of critical areas and damage caused by impact of foreign objects, respectively. Different sensor materials and sizes have been evaluated taking into account both their sensitivity to damage and their embeddability into pre-preg tapes for automatic placement during AFP manufacturing. After testing, flat ribbons (20µm) of CoSiB alloy magnetostrictive sensors and PVDF-TrFE copolymer (Ø6 mm; thickness=40µm) piezoelectric film sensors were selected.

This report gathers a complete description of the sensors, the trials for sensor integration and the evaluation of sensor sensitivity to impacts for the piezoelectric sensor network; to strain for the magnetostrictive sensors; and to temperature variations for both types of sensors.

2. SENSOR SELECTION

Sensor selection is key when designing structural health monitoring systems as they are the first link in the monitoring chain. The type of damage to be detected determines which sensor is the most suitable. In the TOSCA project, magnetostrictive ribbons were pre-selected as the most suitable sensors to provide strain measurements in critical or repaired areas, whereas piezoelectric sensors were pre-selected to provide acoustic signals associated to impact events. In this section, a more detailed analysis on sensor size and material is reported, along with a proof of concept of its detection capability in representative composite laminates.

2.1 Magnetostrictive ribbons

2.1.1 Introduction

Stress-sensitive magnetostrictive wires have been widely studied, and their application in sensors has been proposed[1,2,3]. These applications are mainly based on the large Barkhausen effect, the Matteucci effect and the inverse Wiedemann effect. Other types of amorphous wire microsensors, which are based on the magneto-impedance (MI) effect, have been developed for industrial applications. Original MI sensors that are designed to detect the magnetic field amorphous-wire elements are also sensitive to applied stress[4]. The inverse magnetostrictive effect leads to a change of permeability of wires so that applied stress can change the impedance of the amorphous wires due to the skin effect that occurs with high frequency current excitation as a result of stress dependent impedance change (the stress dependence of giant magneto-impedance effect), great gauge factor has been obtained for CoSiB and CoFeSiB amorphous wires[5]. In addition, the thin form and good mechanical properties of amorphous wires are useful for the attachment of a wire gauge to an elastic element to produce a signal.
It is well known that internal stresses caused by the simultaneous solidification of a metallic nucleus coated with glass lead to a peculiar domain structure. This structure of amorphous microwires consists of an internal axially magnetized core and an outer shell with circular (in the case of a nearly zero magnetostriction constant) or radial (in the case of a positive magnetostriction constant) magnetic anisotropy. It was demonstrated that tensile and torsional stresses modify this domain structure by introducing circular magnetic anisotropy and/or a helically magnetized interface between both areas[6,7,8].

[1] Panina L V, Mohri K, Bushida K and Noda M (1994) "Giant magnetoimpedance and magneto-inductive effects in amorphous alloys" J. Appl. Phys. 76 6198

[2] Zhang H, Zhao Y, Yang S and Li H (1998) "A novel Co-based amorphous magnetic field sensor" Sensors Actuators A 69121–5

[3] Yelon A, Ménard D, Britel M and Ciureanu P (1996) "Calculations of giant magnetoimpedance and of ferromagnetic resonance response are rigorously equivalent" Appl. Phys. Lett. 69 3084

[4] Zhukov, Zhukova V, Blanco J M, Cobeno A F, Vazquez M and Gonzalez J (2003) "Magnetostriction in glass coated magnetic microwires" J. Magn. Magn. Mater. 258–259 151

[5] Uchiyama T, Borza F and Meydan T (2004) "Static torque measurement using gmi strain gauge" J. Optoelectron. Adv. Mater. 6 699–703

[6] Hristoforou E and Reilly R E (1993) "Tensile stress distribution sensors based on amorphous alloys" J. Magn. Magn. Mater. 119 247–53

[7] Hristoforou E, Chiriac H, Neagu M, Darie I and Ovari A (1996) "Torsion and stress in amorphous positive magnetostrictive wires" IEEE Trans. Magn. 32 4953–5

[8] Zhang S L, Sun J F, Xing D W, Qin F X and Peng H X (2011) "Large GMI effect in Co-rich amorphous wire by tensile stress" J. Magn. Magn. Mater. 323 3018–21

Therefore, the spatial magnetization distribution close to the surface is changed. Accordingly, one can expect a change of the magneto-impedance response under the effect of applied tensile and torsion stresses.

The methodology described in the literature involves connecting the magnetostrictive wires to a circuit to measure a response. In the case of a single strain gauge made of such alloys, it is rather easy to employ these methods. However, incorporating a large number of magnetostrictive wires in a structure in the form of a grid, involves practical problems and limitations. One problem arises from the large number of electrodes that are necessary to connect the magnetostrictive wires to the measuring device. Another disadvantage of these methods is the lack of local measurements, because the signal refers to the entire length of the wire, describing the average value of strain.

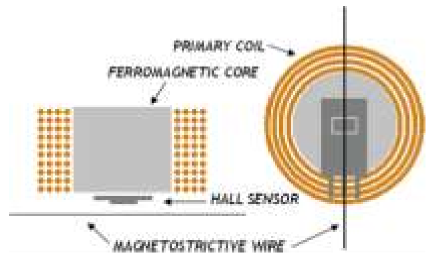

Figure 1. Schematic representation of the circular coil/Hall sensor transducer.

For this project, an inductive technique was developed to simplify the measurement and data acquisition procedure. The basic idea is to use the magnetostrictive sensors as part of a magnetic circuit. The magnetic circuit is completed through the use of an inductive transducer, as illustrated in Figure 1. Direct current is fed to the excitation coil of the transducer to produce a constant magnetic field. Most of the flux will pass through the magnetostrictive ribbons since their permeability is several times larger than the polymeric composite material. The magnetic flux (circulating the circuit) is dependent on the geometry and the magnetic properties of the materials constituting the circuit and it is measured by a Hall effect sensor. Consequently, any change in the magnetic flux reflects the response by the magnetostrictive sensors.

To have a better understanding of the transducer's function, a numerical model has been developed. The model uses the same geometry and physical properties of an actual electromagnet, while the Hall sensor is not included in model's geometry. Figure 2a shows the model's geometry and the magnetic field lines around the transducer. We can also visualize the shape of the magnetic field right below the transducer (Figure 2b), where the inspection area is supposed to be. As illustrated, the distribution of the vertical component of the magnetic flux density is limited within the vicinity of the transducer and could be considered as uniform.

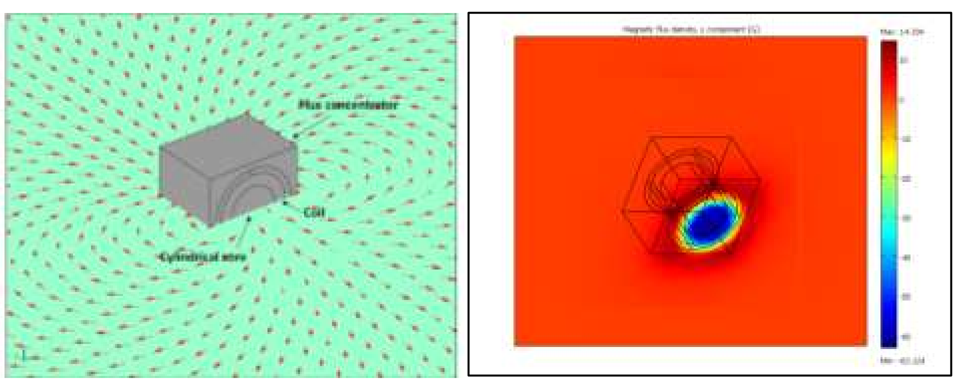

Figure 2. a) The Model's geometry and the magnetic lines around the transducer b) The shape of the magnetic field under the transducer.

2.1.2 Magnetostrictive sensor selection

There are several different alloys characterized as magnetostrictive that could be used for sensor applications. Most common categories are:

Metal-Based Alloys

- Iron (Fe) – moderate magnetostriction, inexpensive
- Nickel (Ni) – relatively small strain sensing
- Cobalt (Co) – used in specialized alloys
- Iron–Silicon alloys (Fe–Si) – improved magnetic properties, used in transformers
- Iron–Cobalt alloys (Fe–Co) – higher saturation magnetization

Rare-Earth Alloys (Giant Magnetostrictive Materials)

- Terfenol-D ($Tb_{0.3}Dy_{0.7}Fe_2$) – the most well-known giant magnetostrictive material
- Galfenol (Fe–Ga alloys) – good ductility and moderate magnetostriction
- Alfenol (Fe–Al alloys) – cheaper and moderate magnetostriction

From the two categories we chose to work with materials from the first group, because the Rare-Earth alloys work better with electrodes rather than an inductive transducer and also, they are much more expensive. In the past GMI have measured the response of FeSiB and CoSiB alloys embedded in carbon fibre laminates[9]. The first has positive magnetostrictive coefficient λ, while the other has a negative magnetostrictive coefficient λ. Based on the results presented in Figure 3, we can see that **CoSiB** alloy has wider sensing range while the response is similar to the FeSiB alloy, so it is more appropriate for our application.

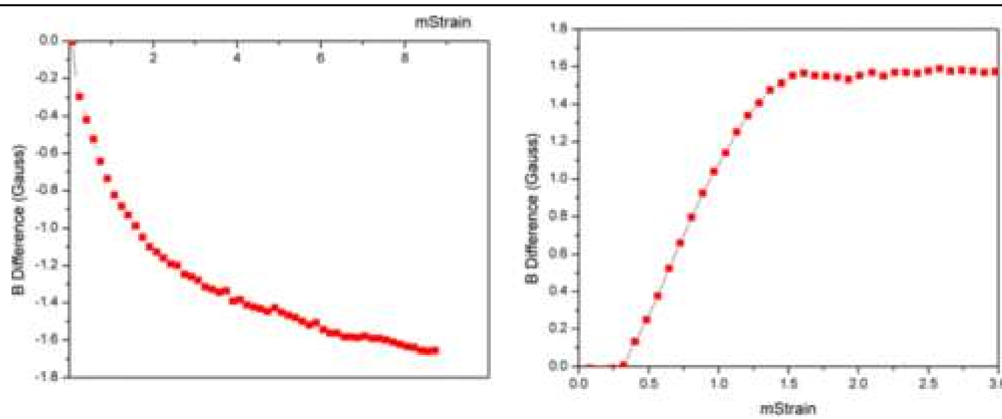

Figure 3. The response of a) CoSiB and b) FeSiB alloys embedded in carbon fiber laminates.

Another categorization can be made on how the magnetostrictive alloys are produced. There are mainly three types:

- Glass covered (average dimeter 50 μm)
- Circular wires (average diameter 100 μm)
- Flat ribbons (thickness 20 μm)

[9] Christopoulos, A., Hristoforou, E., Koulalis, I., Tsamasphyros, G. (2014) "Inductive strain sensing using magnetostrictive wires embedded in carbon fibre laminates", Smart Materials and Structures, 23 (8), art. no. 085035

For this project we selected to work with **flat ribbons** because they are thinner and they could be easier incorporated in composite laminates.

2.1.3 Example: Surface measurements on a composite laminate

To create a sensing patch, the magnetostrictive ribbons are placed in parallel on fiberglass tissue using spray adhesive (FusionFix EP). The magnetostrictive patch is bonded permanently on the composite laminate using Epoxy adhesive, cured in room temperature, as illustrated in Figure 4.

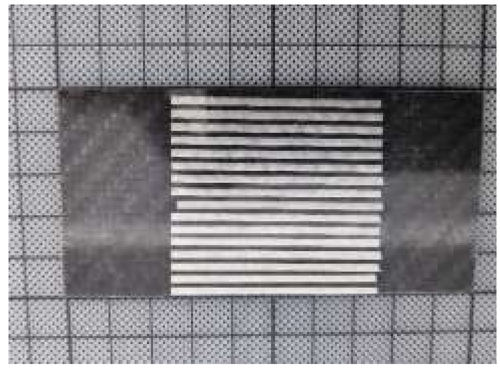

Figure 4. The magnetostrictive patch incorporated in a composite laminate

Local measurements can be obtained using the inductive transducer and a prototype measuring device, that has been developed by GMI and illustrated in Figure 5a. For the moment the measurements represent relative values and not the absolute magnitude of strain. In order to capture surface measurements from the magnetostrictive patch, the inductive transducer is placed on a motorized system that acts like a scanner, illustrated in Figure 5b. The system records the position as well as the output from the transducer. The data are collected and stored on a txt-file from which a 3D graph is generated. Figure 6 shows an example of measurements taken from the surface of the composite laminate.

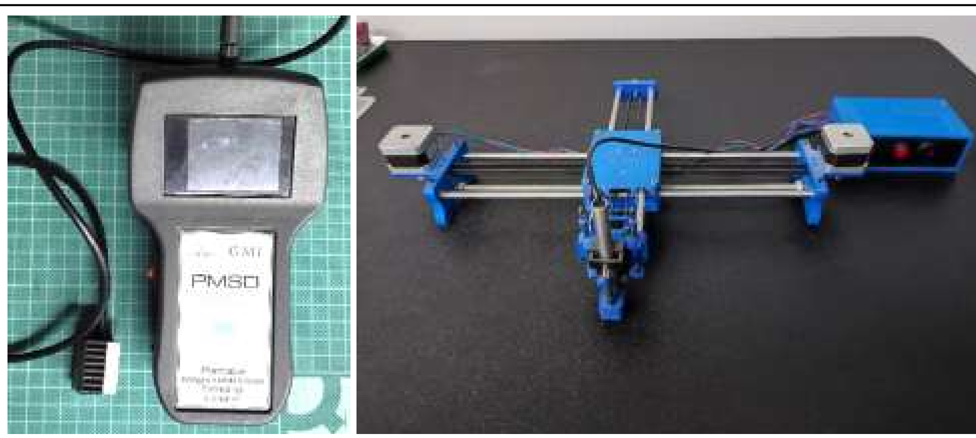

Figure 5. The prototype measuring device b) The motorized system with the transducer.

2.2 Piezoelectric sensors

The proposed methodology for impact detection is based on the acoustic emission (AE) technique. Acoustic Emission is a non-destructive structural health monitoring method that enables real-time detection of elastic energy releases in the form of acoustic waves generated by various damage mechanisms within materials and structures. These mechanisms include crack propagation, plastic deformation processes, impacts, delamination, and other phenomena capable of producing micro-energy releases that can be detected by piezoelectric sensors. Unlike other non-destructive testing (NDT) methods based on point-by-point inspection, AE allows continuous monitoring, covers large areas with a relatively small number of sensors, and can detect dynamic events that other techniques cannot capture. This makes it particularly valuable in sectors such as aeronautics, wind energy, civil infrastructure, and pressure vessels.

An Acoustic Emission system is designed to detect, amplify, record, and analyze elastic waves generated by dynamic events in a structure. To achieve this objective, the first stage involves the selection and

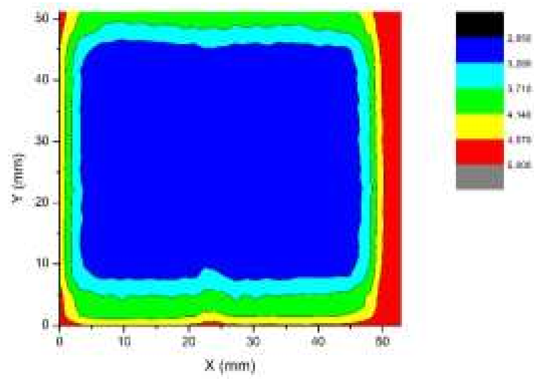

Figure 6. Example of measurements taken from the surface of the composite laminate. Colour scale in Volts (V)

configuration of the hardware components of the system, including choosing the most suitable transducers for embedding during the CFRP part manufacturing process.

The first constraint is a physical one. The sensor dimensions are limited by the AFP tape width (approximately 0.5”), therefore each sensor type has been selected—within the range of sizes offered by each manufacturer—to ensure a maximum width well below 10 mm. This avoids any risk of tape entanglement caused by the sensors placed on top of the tape prior to manufacturing. Sensor thickness has not been considered an issue, since typical values are below one millimetre, which is acceptable and does not interfere with the AFP process.

The second constraint concerns the AE characteristics of each specific sensor. Considering that the voltage output of a piezoelectric device—when through-thickness polarized and operating in radial coupling mode for shear-wave sensing—is proportional to its thickness and inversely proportional to its capacitance, a trade-off must be established. High voltage outputs are expected when dealing with high-energy impacts occurring close to the transducer. However, the signal must also remain above the inherent electrical noise of the measurement chain in order to detect far-field or ultra-low-energy events.

The third constraint is process temperatures, since piezoelectric effects disappear once the material temperature rises above the Curie temperature (which induces depolarization). Additionally, exposure to temperatures above 80 °C for extended periods of time may cause shrinkage in PVDF materials, resulting in changes to the final sensor dimensions.

Considering all constraints, three different types of sensor transducers have been evaluated: traditional piezoceramics, PVDF piezoelectric films, and PVDF-TrFE printed films. Piezoceramic transducers are well-established for AE sensing due to their high sensitivity and low cost. However, ceramic materials tend to be brittle, which is why flexible sensors have also been considered to evaluate their suitability for integration into the manufacturing process. The selected sensors are presented in Table 1, and their main characteristics are summarized in Table 2.

Piezo Ceramic Disc	PVDF-TrFE	PVDF piezoelectric
		

Table 1: Sensor typologies evaluated for embedding while manufacturing using AFP

Manufacturer	Manufacturer reference	Description	Diameter [mm]	Thickness [mm]	Capacitance [nF]	d_{33} [C/N]	ε_r	Unit price [€]
Steiner and Martins Inc.	SMD07T02S412	Piezo Ceramic Disc	7	0.2	1.6	$4.5\cdot10^{-10}$	1850	2.5
PolyK Technologies, LLC	F2325-40um-8	PVDF-TrFE Copolymer piezoelectric film ultrasound transducer	6	$40\cdot10^{-3}$	30	$3.0\cdot10^{-11}$	8.3	7.9
PolyK Technologies, LLC	PKS-T110- D020-10-6M	PVDF piezoelectric film ultrasound transducer	6	$110\cdot10^{-3}$	29	$2.8\cdot10^{-11}$	13.5	15.6

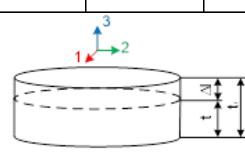

Table 2. Characteristics of the evaluated sensors

For lead zirconate titanate (PZT) discs used as AE sensors, a simple way to compare voltage output for the same mechanical input is to use the piezoelectric and mechanical properties and geometry; this allows to rank different discs without fully modelling the structure. For in-plane acoustic emission (AE) sensing with piezoelectric films like PVDF and PVDF-TrFE, the expected signal amplitude comes from how in-plane strain couples into an electric field through d_{31}. For a thin film poled through thickness (direction 3):

$$D_3 = d_{31}\,\sigma_1 + \varepsilon_{33}E_3$$

Where D_3 is the electrical displacement in the thickness direction, d_{31} represents the in-plane piezoelectric coupling effect, $\varepsilon_{33}$is the dielectric permittivity measured at zero mechanical stress, $\sigma_1$is the in-plane stress and E_3 is the through thickness electric field. Under open circuit conditions:

$$E_3 = -\frac{d_{31}}{\varepsilon_{33}}\,\sigma_1 \tag{1}$$

Voltage across thickness t:

$$V = E_3\,t = -\frac{d_{31}}{\varepsilon_{33}}\,\sigma_1\,t \tag{2}$$

Using $\sigma_1 = \frac{\varepsilon_1}{s_{11}}$ where s_{11} is the in-plane compliance and ε_1 the in-plane strain

$$V = -\frac{d_{31}}{\varepsilon_{33}\, s_{11}}\, \varepsilon_1\, t \tag{3}$$

For several transducers bonded similarly to the structure and excited by the same AE source, assuming similar strain at the disc–structure interface for comparison, then relative sensitivity in dB between transducer *i* and *j* is:

$$S_{i/j}[dB] \approx 20log_{10}\left(\frac{d_{31}^{i} t^{i}\ \varepsilon_{33}^{j} s_{11}^{j}}{d_{31}^{j} t^{j}\ \varepsilon_{33}^{i} s_{11}^{i}}\right) \tag{4}$$

For the PVDF and PVDF-TrFE materials the typical value of piezo coefficients are 20 and 35 pC/N and the in-plane compliance about and 4 and 5·10-10 Pa-1 respectively. Considering as reference the piezoceramic disc, the relative sensitivities for the PVDT TrFE is -11.5 dB and for the PVDF -13 dB, meaning that the voltage output for the PVDF transducers will be about 4 times lower than the piezoceramic disc. Considering the relative sensitivity among the investigated sensors, the thermal stability (up to 125º C in the case of the PVDF-TrFE material), the individual cost and prioritizing a flexible sensor for easing the integration in the manufacturing process the selected sensors is the PVDF-TrFE Copolymer piezoelectric film ultrasound transducer.

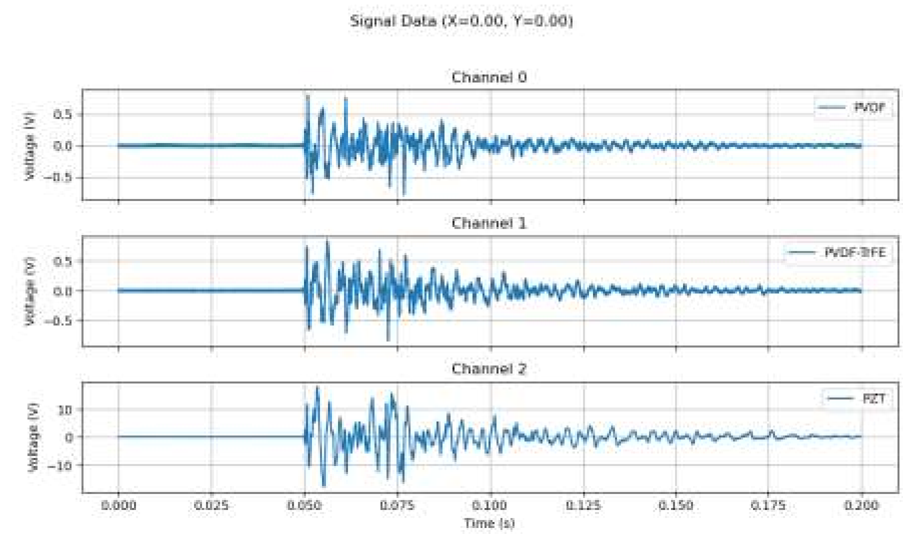

Figure 7. Example of voltage output for the selected transducers. 1J impact on a CFRP plate at 250 mm from the sensor location, with equivalent orientations.

Finally, an example of the voltage output for each sensor is shown in Figure 7. A controlled energy impact abut 1J is applied to the centre of the plate and registered using the different type of chosen sensors located on the plate at 250 mm from the point of impact. By analysing the envelope of the voltage output for each sensor, and extracting their peak values, it is observed that the piezoceramic transducer produces a voltage approximately 20 times higher for the same quantified impact. This suggests that the material properties assumed for the PVDF sensors may not be sufficiently accurate, a combination of in-plane and through thickness excitation is present or that the bonding between the sensors and the plate surface was not fully optimal. Anyway, both PVDF sensors exhibit similar voltage levels; therefore, the more economical option is selected for the next stages of the project.

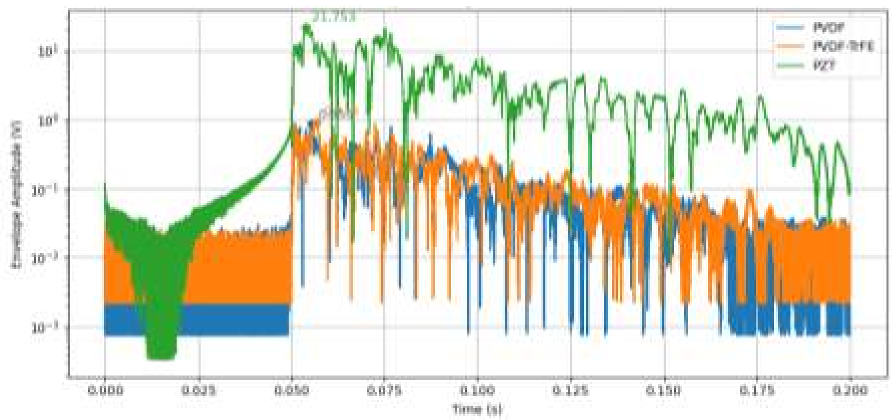

Figure 8. Comparison of the voltage output envelope for the selected transducers. 1J at 250 mm from the sensor location.

3. SENSOR INTEGRATION

The sensor network can be either surface mounted using adhesives or embedded into the composite laminate. While surface mounted sensors are easy to attach with no disturbance on either the laminate or the sensor behaviour, the use of adhesives adds uncertainties on the measurements and weakens the robustness of the solution. On the contrary, embedded sensors provides higher robustness of the network and avoid the use of adhesives, delivering “smart” components. However, this does not come without drawbacks. How to perform the electrical connections of embedded sensors, how the mechanical performance of the laminate will be affected by embedded objects and sensor survivability related to the manufacturing process (temperature and pressure) are some of the main challenges.

The sensor embedding approach follows the sequential manufacturing strategy defined for TOSCA, consisting of three stages:

1. Preform manufacturing: The composite laminate is first laid up using the AFP process with standard (non-instrumented) prepreg tapes.
2. Curing: The preform undergoes a standard curing cycle at 180 °C.
3. Smart layer placement: A final “smart layer” containing the embedded sensors is deposited onto the cured laminate using AFP at a reduced temperature of up to 110 °C.

This sequential approach serves two purposes: it avoids exposing the sensors to the full curing temperature (which could compromise sensor functionality), and it prevents embedded sensors from acting as damage initiators within the structural laminate.

In this section a description of the embedding process into the tapes and its use for AFP manufacturing is reported along with the verification of sensor behaviour after the manufacturing process.

3.1 Magnetostrictive Ribbons

3.1.1 Sensor Description

The magnetostrictive ribbon sensors used in TOSCA are supplied by GMI Aero (France). These sensors are designed as thin, flexible metallic ribbons that exploit the magnetostrictive effect to detect strain variations in the host composite structure. Their ribbon geometry makes them particularly well-suited for integration into narrow prepreg tape formats, as they can be cut to length and conform to the half-inch (12.7 mm) tape width used by the AFP-XS system without exceeding the channel width of the placement head.

3.1.2 Embedding Approach

For the initial integration trials conducted at AddComposites the magnetostrictive ribbons were placed onto vitrimer-based prepreg tape supplied by CIDETEC. The embedding procedure was as follows:

- The vitrimer tape surface was heated using an external hot air gun to activate the resin tack (approximately 70–90 °C).
- The magnetostrictive ribbon was positioned on the heated tape surface and pressed into place while the tape was tacky.
- The instrumented tape was then loaded into the AFP-XS head and deposited through the standard automated placement process.

The magnetostrictive ribbon passed through the AFP-XS placement head without mechanical damage and was successfully deposited onto the substrate. Visual inspection of the placed tape confirmed that the ribbon conformed to the tape surface and remained well-bonded throughout the placement sequence.

In parallel, GMI Aero prepared sensor-integrated tapes at their facility using the same heat-activated tack approach. By January 2026, GMI had completed a 2.5-metre tape spool with integrated magnetostrictive sensors, which was shipped to FIDAMC for automated deposition and curing validation trials.

3.1.3 Observations and Current Limitations

The magnetostrictive ribbon demonstrated favourable embeddability characteristics due to its thin, flexible metallic structure. Unlike the piezoelectric sensors (see Section 3.2), the ribbon does not have protruding connectors that could interfere with the tape guidance channel, and its flexibility allows it to conform to moderate curvatures during placement.

The following limitations and open points have been identified:

- Functional verification pending: Visual inspection confirmed satisfactory bonding of the ribbon to the tape surface after AFP placement. However, quantitative assessment of the bond quality between the metallic ribbon and the vitrimer matrix — and verification that the sensor retains its strain sensitivity after the embedding process — is being conducted by GMI Aero using the 2.5 m integrated tape shipped to FIDAMC. Preliminary results are shown below and further results are expected in the M18–M24 period.
- Substrate quality variability: The initial tapes received from CIDETEC were from an early production batch and exhibited a relatively dry surface with powder residue from the release film used during slitting. This may have reduced the effective resin tack available for bonding the sensor to the tape. Newer tapes with improved resin content have since been received from CIDETEC, and optimisation trials using these tapes are planned prior to M18.
- Process parameter optimisation: The temperature and speed settings during the smart layer placement influence the degree of tack activation and, consequently, the bond quality between the sensor and the substrate. Systematic optimisation of these parameters for sensor-embedded tapes is ongoing, using the recently received CIDETEC tapes.

3.1.4 Comparison: Embedded Vs. Surface Mounted

The embedded sensor specimens from the current trials have been sent to GMI Aero for functional characterisation. Incorporating the magnetostrictive ribbons during the curing of the composite laminate offers very strong bonding between the sensors and the composite laminate but induces an offset on the measurements, mainly due to:

- residual stresses that occur after the curing cycle because of the mismatch of the thermal expansion coefficient of the alloy and the composite.

- annealing during the curing cycle, that leads to rearrangement of the magnetic domains of the alloy and consequently affecting its magnetic properties.

On the other hand, an adhesive bond does not induce an offset but offers a weaker bond. In Figure 9, a comparison of the two methods of integration is presented. A direct quantitative comparison between embedded and surface-mounted magnetostrictive sensor response is not yet available and will be addressed in subsequent work. The key anticipated advantage of the embedded configuration is improved robustness of the sensor network: embedded sensors are protected from mechanical damage during service and do not rely on adhesive bonds that may degrade over time under environmental exposure. The principal trade-off is the added complexity of electrical connections, which must be routed from the embedded sensor position to the exterior of the laminate without compromising structural integrity.

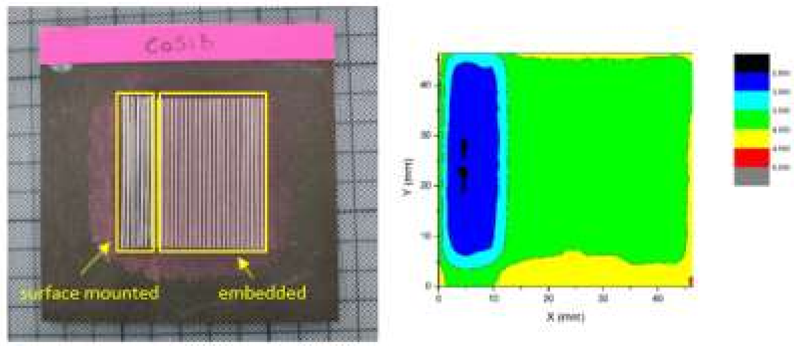

Figure 9. Comparison of surface mounted vs embedded on the response of the transducer.

3.2 Piezoelectric sensors

3.2.1 Sensor Description and Selection

ITA (Instituto Tecnológico de Aragón) supplied three types of piezoelectric sensor candidates for evaluation as detailed in Table 1:

- Ceramic PZT sensor — a rigid piezoceramic element.
- PVDF sensor with silver electrodes — a flexible polymeric sensor with conventional wire connectors.
- PVDF-TrFE sensor with gold electrodes — a flexible polymeric sensor with a thin-film electrode configuration.

The selection of the most suitable sensor for AFP integration was based on embeddability criteria, assessed through lay-up trials conducted at Addcomposites during the M7–M12 period. Each sensor type was tested in the AFP-XS placement head to evaluate its compatibility with the automated manufacturing process.
Ceramic PZT sensor: This sensor was discarded early in the evaluation. The rigid ceramic element proved too fragile for the AFP manufacturing process. During lay-up trials, the sensor fractured under the mechanical forces exerted by the compaction roller and tape guidance system. The brittleness of the ceramic substrate makes it incompatible with the bending and pressure loads inherent to automated tape placement.
PVDF sensor with silver electrodes: This sensor was tested in the AFP-XS head but proved incompatible. Its wire connectors were bulky and protruded beyond the half-inch tape width. During the placement trial, the sensor became lodged in the AFP-XS head’s tape guidance channel (12.7 mm width) and was stripped from the tape. The connector geometry makes this sensor type unsuitable for automated placement without significant redesign of the electrical connections.
PVDF-TrFE sensor with gold electrodes: This sensor was identified as the best candidate for AFP integration. Its thin-film gold electrode structure is compatible with the tape dimensions, and the flexible PVDF

substrate can conform to the placement path without fracturing. This sensor type was selected for further integration trials.

3.2.2 Embedding Process

The embedding procedure for the gold-electrode PVDF sensors followed the same sequential manufacturing approach as described for the magnetostrictive ribbons (Section 3.1). The sensor was placed onto vitrimer prepreg tape using heat-activated tack, without additional adhesive:

- A hot air gun was used to raise the vitrimer tape surface temperature to approximately 70–90 °C, activating the resin tack.
- The gold-electrode PVDF sensor was manually positioned on the heated tape surface and pressed into contact.
- No additional adhesive, epoxy, or bonding agent was applied.
- The instrumented tape was loaded into the AFP-XS head and deposited through the automated placement process.

The sensor passed through the AFP head and was deposited onto the substrate without mechanical damage. The lay-up process itself (feeding, guiding, compaction) was completed successfully, demonstrating that the sensor geometry is compatible with the AFP-XS placement mechanism.

3.2.3 Bonding Assessment and Challenges

Following the integration trials, the sensor-embedded coupons were shipped to ITA for functional characterisation. Testing revealed that the gold-electrode PVDF sensor was not adequately bonded to the composite substrate and peeled off from the substrate. While the sensor remained in position during lay-up (suggesting sufficient initial tack for handling), it was not firmly attached, and functional measurements indicated insufficient strain transfer from the substrate to the sensor.
The following root causes were identified in a dedicated bilateral meeting between Addcomposites, ITA, and GMI Aero:
Tape surface condition: The initial batch of vitrimer tapes from CIDETEC exhibited a dry surface with powder residue from the release film used during the slitting process. This reduced the available resin tack and may have prevented adequate wetting of the sensor surface during embedding.
Metallic sensor surface: The gold electrode presents a metallic surface that may require specific surface preparation (degreasing, light abrasion) or a dedicated adhesive interlayer to achieve a reliable bond with the vitrimer matrix. ITA's standard procedure for surface-mounting these sensors involves light grinding of the composite surface followed by cyanoacrylate adhesive bonding.
Absence of adhesive: No additional bonding agent was used in the initial trials. The reliance on resin tack alone proved to be insufficient for this sensor type. However, the use of cyanoacrylate adhesive (as employed by ITA for surface mounting) is not viable for embedded sensors, as cyanoacrylate degrades at approximately 80 °C — below the processing temperature required for the smart layer placement step (up to 110 °C).

3.2.4 Planned Improvements

Based on the analysis of the initial trial results, the following corrective actions have been defined and are being implemented:

- Use of newer prepreg tapes: Subsequent trials will use freshly produced vitrimer tapes with higher resin content from CIDETEC, which are expected to provide improved surface tack for sensor bonding. These tapes have been received and are available for the next trial campaign.
- Process parameter optimisation: The AFP placement parameters (heater power, lay-up speed, compaction force) will be systematically varied to identify conditions that maximise the bond quality between the sensor and the vitrimer tape. The focus will be on increasing the resin activation temperature while remaining below the sensor depolarisation threshold.

- Alternative bonding strategy: If resin tack alone remains insufficient, a high-temperature-resistant adhesive will be evaluated as an interlayer between the sensor and the tape. The adhesive must withstand the smart layer placement temperature (up to 110 °C) without degradation. Identification and sourcing of a suitable high-temperature adhesive is ongoing.
- Sensor redesign for electrical connections: ITA is preparing a new batch of 4 to 10 sensors with integrated wiring. The current sensors lack wiring on the bottom contact point, which prevents functionality testing when the sensor is embedded (face-down) in the tape. The new batch will use the same-thickness conductive film for wiring, maintaining the original sensor footprint within the half-inch tape width while enabling post-embedding functional verification.
- Trial timeline: Refined sensor integration trials are planned for May–June 2026, using the AFP tool at Addcomposites' facility in Helsinki. A cured laminate will first be prepared (by AFP or hand lay-up), and the smart layer with embedded sensors will then be placed on top to validate the bonding of the instrumented layer to the cured substrate. Updated results from these trials will be reported in Deliverable D5.1.

3.2.5 Limitations of the Piezoelectric Sensor Approach

The principal challenges identified for piezoelectric sensor embedding via AFP are:

- Depolarisation risk: PVDF sensors may lose their piezoelectric properties if exposed to temperatures exceeding their Curie temperature during the manufacturing process. The sequential manufacturing approach (smart layer applied after curing) mitigates this risk by limiting the sensor exposure to approximately 110 °C rather than the full 180 °C curing cycle.
- Shrinkage of polymeric substrate: The PVDF film may undergo dimensional changes during thermal exposure, potentially affecting the sensor calibration and the mechanical coupling between the sensor and the host laminate.
- Bonding reliability: As demonstrated in the initial trials, achieving a reliable bond between the metallic sensor surface and the vitrimer tape matrix requires further process development. The bonding mechanism must be robust enough to ensure adequate strain transfer for SHM functionality throughout the service life of the structure.
- Electrical connection routing: Embedded sensors require electrical connections to be routed from within the laminate to the exterior. The wiring must fit within the half-inch tape width and must not introduce stress concentrations or delamination initiation sites in the laminate. ITA's planned solution — using same-thickness conductive film — is designed to address this constraint.

3.3 Summary and Outlook

Sensor Type	AFP Compatibility	Bonding Quality	Functional Verification	Status
Magnetostrictive ribbon (GMI Aero)	Passed	Visually satisfactory	Pending (GMI testing)	Successful integration
Ceramic PZT (ITA)	Failed — fractured	N/A	N/A	Discarded
PVDF silver electrodes (ITA)	Failed — stuck in head	N/A	N/A	Discarded
PVDF gold electrodes (ITA)	Passed	Insufficient (first trial)	Not functional (unbonded)	Under improvement

Table 3. Current status of sensor integration.

The initial integration trials have established two important results:

- The AFP-XS system is mechanically capable of placing sensor-embedded tapes. Both the magnetostrictive ribbon and gold-electrode PVDF sensor passed through the automated placement process without damage, confirming that the AFP head geometry and process forces are compatible with sensor integration when the sensor dimensions respect the half-inch tape width constraint.

- Reliable sensor-to-tape bonding requires further development. The magnetostrictive ribbon showed promising bonding behaviour (visual inspection confirmed good adhesion), while the PVDF sensor bonding was insufficient when relying on vitrimer resin tack alone. The root causes — early-batch tape dryness and the metallic sensor surface — have been identified, and corrective actions are in progress.

The following activities are planned to address the bonding challenge and complete the sensor integration validation:

1. Optimisation trials with CIDETEC's improved vitrimer tapes (higher resin content) — planned for May–June 2026.
2. Systematic variation of AFP process parameters (temperature, speed, compaction force) for sensor-embedded tapes.
3. Evaluation of high-temperature adhesive interlayer if resin tack optimisation alone proves insufficient.
4. Integration trials with ITA's new sensor batch featuring integrated thin-film wiring.
5. Functional characterisation of embedded sensors (strain sensitivity, frequency response) in collaboration with ITA.
6. Comparison of embedded vs. surface-mounted sensor performance for both sensor types.

Updated results from these activities will be reported in Deliverable D5.1.

4. SENSOR SENSITIVITY

The sensitivity of a sensor refers to its ability to detect and respond to changes in the measured quantity, and it determines the smallest measurable signal change. While higher sensitivity improves resolution and the signal-to-noise ratio, it often causes the sensor to saturate earlier, reducing its maximum operational range. In TOSCA, the sensitivity of magnetostrictive sensors to changes in strain and the piezoelectric sensor sensitivity to impact energy were evaluated having into account the operational range needed. Additionally, the sensitivity of both sensors to the mentioned changes is evaluated under different temperature operational conditions to ensure robustness of the system.

4.1 Sensitivity to deformations

In this section the sensitivity and the ability of damage detection of the proposed methodology is presented. In the first set of experiments the magnetostrictive patch is used to detect the location and size of damage caused by impact. For the initial tests the samples are prepared using commercial grade composite laminates (Carbon/Epoxy) in order to save 3R resin, since the composition of the thermosetting resin does not affect the performance of inspection. The intention is to obtain an overview of the range of parameters (energy level, patch size etc.) and the apply them to the actual test samples made from 3R vitrimer resin.

For the fabrication of the test samples the magnetostrictive patch is bonded on the surface of the carbon fibre laminates. The magnetostrictive ribbons are placed in parallel on a thin fiberglass tissue and bonded using epoxy resin which is cured at room temperature, as illustrated in Figure 10.

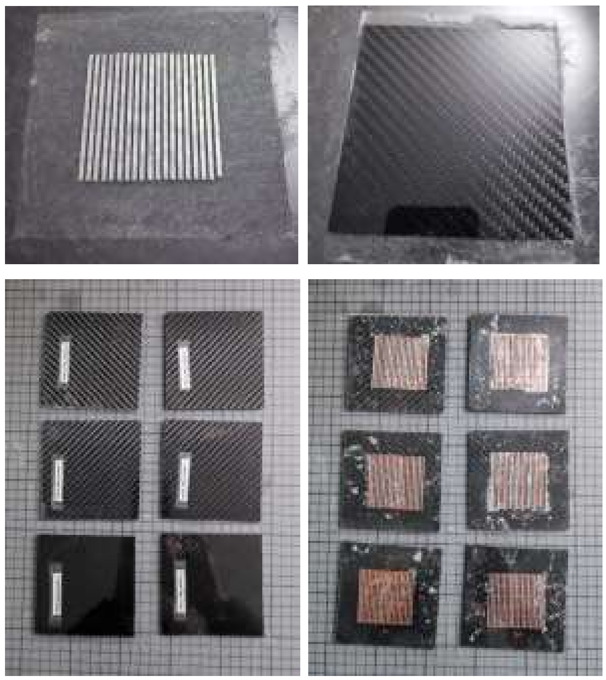

Figure 10. Integration of magnetostrictive patch on the surface of composite laminates

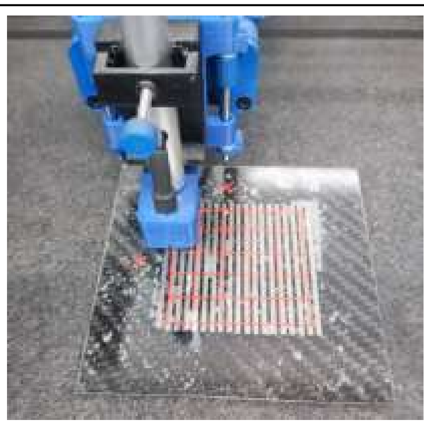

Figure 11. Magnetostrictive inspection using the motorised system.

After the fabrication of the samples, inspection is carried out using ultrasonic testing (A scan) and also scanning by a motorized system. The inspection area is a rectangular of 5x5 cm divided by 1x1 cm grid and it is marked on the surface of the samples using a red marker, as illustrated in Figure 11.

Figure 12. Drop weight impact testing at different energy levels (3, 6 and 9 Joules).

The samples are subjected to drop weight impact testing on the facilities of ITA, as illustrated in Figure 12. The energy levels are selected to be 3, 6 and 9 Joules and two samples are tested for each energy level. Visual inspection after the impact reveals different level of damage at the front and back surface of the samples which is in line with the expected outcome. In Table 4 visual observations are presented for each sample. The samples are inspected again using ultrasonics (A scan) and also scanned by the motorized system. The comparative results from the ultrasonic inspection and the magnetostrictive patch, before and after impact, are presented in Figure 13 and Figure 15 respectively.

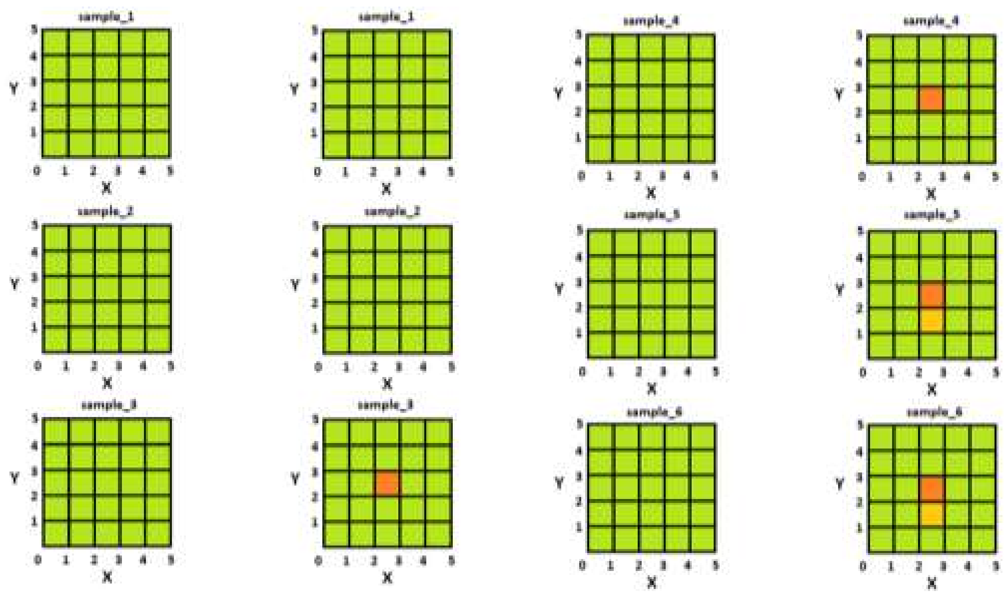

Figure 13. Inspection using ultrasonics A-scan before (left) impact after (right) impact for each sample. Only one side is shown

Sample ID	Impact Energy	Front side	Back side
1	3 J	No visual damage	No visual damage
2	3 J	Small dent	No visual damage
3	6 J	No visual damage	Fiber breakage (medium size)
4	6 J	No visual damage	Fiber breakage (small size)
5	9 J	Small dent	Fiber breakage (large size)
6	9 J	No visual damage	Fiber breakage (large size)

Table 4. Visual inspection after the impact.

The ultrasonic inspection clearly shows that there is damage at the center of samples 3,4,5 and 6. In contrast the samples 1 and 2 do not show any damage. In case of samples 5 and 6 the size of the damage is larger compared to samples 3 and 4. In Figure 14 the waveform of the ultrasonic transducer over the damaged area is presented. Based on the form of the waveforms, the type of damage can be considered as fibre breakage while no delamination is observed in all cases.

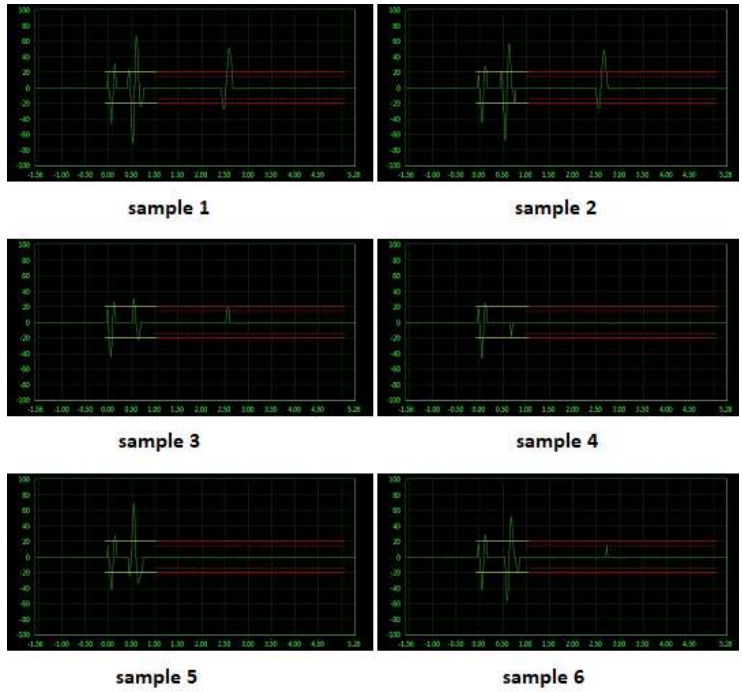

Figure 14. The waveform of the ultrasonic transducer over the damaged area.

From the images taken using the motorized system over the magnetostrictive patch, there are observable differences between undamaged and damaged samples. In the case of damaged samples there is a large deviation from the original measurements in certain locations at the centre. These locations coincide with the location of the damage identified by the ultrasonic inspection. In Figure 15 the results of the inspection before (on the left) and after the impact (on the right) are presented.

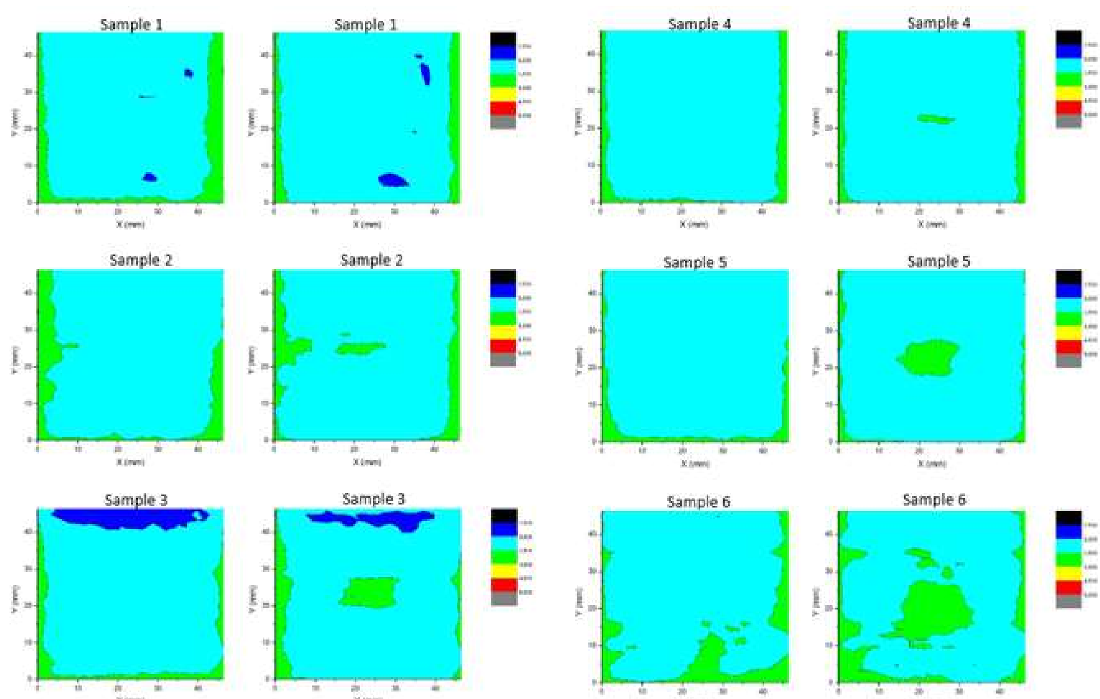

Figure 15. Comparative results before (on the left) and after the impact (on the right).

4.2 Sensitivity to impacts

Acoustic emission monitoring has become a cornerstone technique for real-time structural health assessment, particularly for detecting and localizing impact-induced damage in composite and metallic structures. Among available sensing technologies, PVDF-based sensors represent a compelling alternative to conventional piezoceramic transducers due to their flexibility, low acoustic-impedance mismatch with the host structure, and broad frequency bandwidth. However, their comparatively lower piezoelectric sensitivity introduces challenges for reliable impact localization, especially in noisy environments or when monitoring low-energy impact events.

Quantifying the sensitivity of PVDF-based acoustic emission sensors to impact events is therefore essential to evaluate their suitability for structural health-monitoring applications. Unlike traditional calibration methods that define sensitivity in terms of pressure or displacement, impact-driven scenarios require a metric that directly correlates the sensor’s electrical output with the mechanical energy of the impact. To this end, a standardized procedure for characterizing PVDF-TrFE sensor sensitivity, expressed in volts per millijoule (V/mJ), is developed using controlled drop-weight impacts. This method enables reproducible assessment of sensor performance across different configurations and provides a practical reference for comparing PVDF sensors with alternative transducer technologies, as well as for optimizing their deployment in impact-localization tasks.

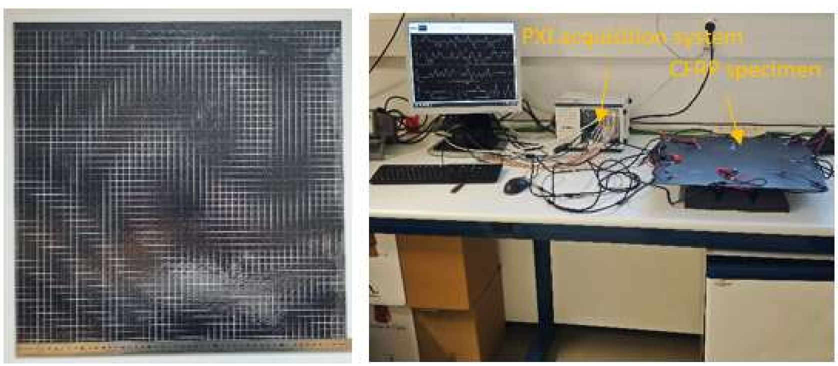

Figure 16. General view of the grid pattern on the sample used to identify the impact location and general view of the test setup.

The procedure established to characterize PVDF sensor sensitivity quantifies the voltage generated by a PVDF-based acoustic emission sensor per unit of impact energy (V/mJ), allowing direct comparison across sensor types and installation locations. The experimental setup comprises the CFRP specimen, the sensing network, the impact source, and the data-acquisition system. A brief description of each element is provided below. A general overview of the specimen and the test configuration is shown in Figure 16.

A CFRP specimen was selected in line with the project objectives, aiming at assessing the capability to detect impact events in representative composite structures. As the final project material was not available at the time of the testing campaign described in this report, a dedicated coupon was manufactured by ITA to characterize the behaviour of PVDF-based sensors when bonded to a CFRP substrate.

The specimen, manufactured with a commercial woven fabric (G0926 5H from Hexcel), consists of a square plate with dimensions 0.5 m × 0.5 m, and a stacking sequence of 6 layers laid-up according to following orientations [0/+45/−45/−45/+45/0]. A nominal thickness of 2.4 mm (2.5 mm for the currently manufactured plate) was obtained. The mechanical properties of the G0926 lamina are provided in Table 5.

E_1 [MPa]	E_2 [MPa]	E_3 [MPa]	ν_{12}	ν_{13}	ν_{23}	G_{12} [MPa]	G_{13} [MPa]	G_{23} [MPa]	ρ [kg/m^3]	Thickness [mm]
59.54	54.95	8	0.03	0.4	0.4	5.21	3.5	3.5	1520	0.41

Table 5. Lamina orthotropic mechanical properties for G0926 material

The PVDF-based sensors are evaluated in terms of the voltage amplitude generated in response to controlled impact events at different locations on the CFRP plate. Although a preliminary selection based on unit cost had already been made, both PVDF and PVDF-TrFE sensors were available. Therefore, a comparative evaluation between the two technologies was included to assess their relative performance and to confirm the initial sensor selection.

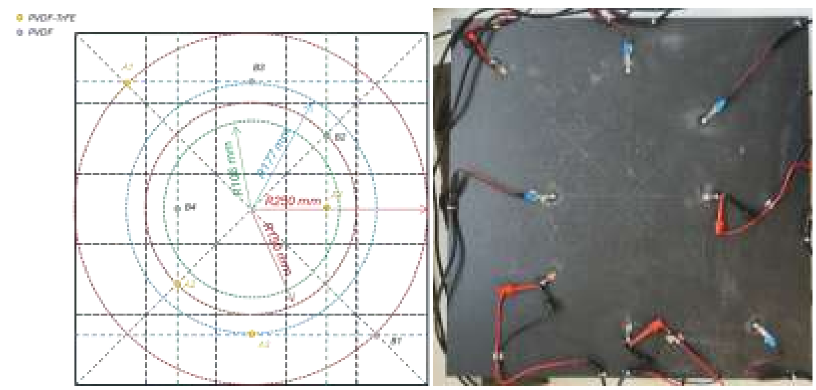

Figure 17. Sensor network configuration (left) and instrumented CFRP specimen (right).

The sensing network topology and the actual specimen configuration are shown in Figure 17. Symmetric sensor locations were defined over the full plate area, considering a range of distances and orientations with respect to the plate centre. These orientations were selected to account for laminate orthotropy. For each nominal distance, PVDF and PVDF-TrFE sensors were placed at equivalent positions to enable direct comparison.

All PVDF-based sensors were bonded to the CFRP surface using a thin layer of cyanoacrylate adhesive (Loctite 401). The bonding procedure included a surface preparation process consisting of cleaning, degreasing and light sanding of the plate surface in the sensor area. After bonding, the sensors were covered with HBM SG250 silicone rubber to protect the installation.

A calibrated drop-weight impactor was used as the source of mechanical excitation. The impactor consists of a semi-spherical steel tip with a diameter of 19.75 mm, and a guiding body with a total combined mass of 998.06 g. The drop height is continuously adjustable by means of a locking–releasing ring mechanism, which allows setting the desired impact energy by selecting the height prior to the test. Figure 18 shows details of the impactor tip and the locking–releasing system.

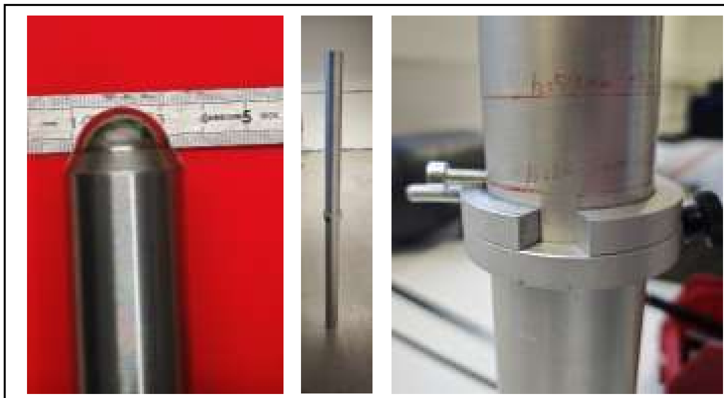

Figure 18 Detail of the impactor tip (left), free-fall apparatus used in the controlled energy tests (center) and impactor locking and releasing mechanism (right).

Three impact energy levels were considered in the experimental campaign: 0.25 J, 0.5 J and 1 J. The maximum energy level was chosen conservatively to avoid any damage in the CFRP specimen, which is currently the only coupon available for development purposes.

The data acquisition system (DAQ) consists of an NI PXIe-1071 chassis equipped with an NI PXIe-8861 embedded controller, and three NI PXI-5105 oscilloscopes, each providing eight channels. Eight channels are used simultaneously to record the voltage output of the AE sensors. The main acquisition specifications and parameters are summarized in Table 7 and Table 6. These parameters were selected primarily to ensure a sufficient number of samples per event to accurately estimate the signal energy content and reduce the total volume of recorded data to a manageable level. The selected sampling frequency is relatively low compared with typical acoustic emission applications. However, it is considered adequate for the intended purpose, since no advanced frequency-domain processing of the time series is anticipated at this stage.

Category	Specification
Bandwidth	60 MHz
Analog channels	8 channels, simultaneous sampling
Resolution	12 bits
Sampling rate	60 MS/s (per channel)
Connectors	SMB
Input impedance	50 Ω ±2% or 1 MΩ ±1% (50 pF)
Coupling	AC or DC (AC available only on 1 MΩ input in PXIe; both available in PXI)
Input ranges	0.05 V, 0.2 V, 1 V, 6 V (50 Ω and 1 MΩ) / 30 V (1 MΩ only)
Maximum overvoltage	50 Ω: 7 Vrms, peaks ≤10 V — 1 MΩ: peaks ≤42 V
DC accuracy	Between ±(1% × reading + 0.25% FS + 600 µV) and ±(0.65% × reading + 0.25% FS + 600 µV), depending on range
AC accuracy	50 Ω: ±0.1 dB • 1 MΩ: between ±0.13 and ±0.4 dB depending on range
Memory	512 Mpts
Input type	Referenced single-ended
Sample clock	60 MS/s, PLL-synchronization compatible
Operating temp.	0 °C to 55 °C
Required calibration	External calibration at 23 °C ±3 °C

Table 6. Specifications of the DAQ system used in the AE tests

Sample rate [Samples/s]	1.000.000
Coupling	DC
Save window [Samples]	200.000 (20% pre-impact)
Trigger threshold [V]	0.1

Table 7. AE system configuration

The nominal impact energy is calculated according to the next expression

$$E = m \cdot g \cdot h \text{[J]}$$

where $g = 9.81$ m/s^2, and the electrical voltage output is estimated as:

$$A_{\max} = \max_t \left(\sqrt{V(t)^2 + (\mathcal{H}\{V(t)\})^2} \right)$$

The sensor voltage time series is denoted by $V(t)$. The signal envelope is obtained via the Hilbert transform $\mathcal{H}\{V(t)\}$.

A comprehensive test plan was executed, combining impacts at the plate centre, and the three predefined energy levels (0.25 J, 0.5 J and 1 J). Since the sensing network includes multiple distances and orientations relative to the plate centre, the effect of distance on the sensor sensitivity is explicitly considered. For each impact location, five repetitions were performed to capture statistical variability.

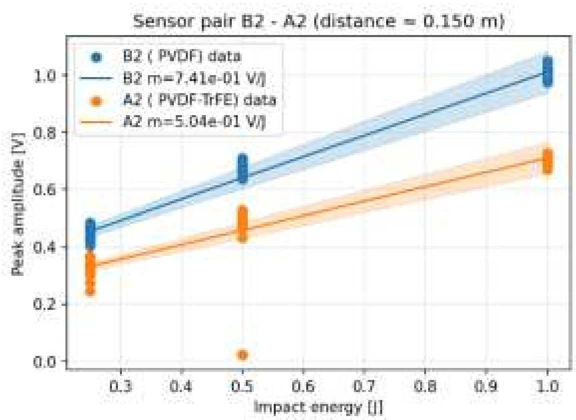

Figure 19. Sensitivity for PVDF-based sensors at 150 mm form the point of impact and +45º orientation.

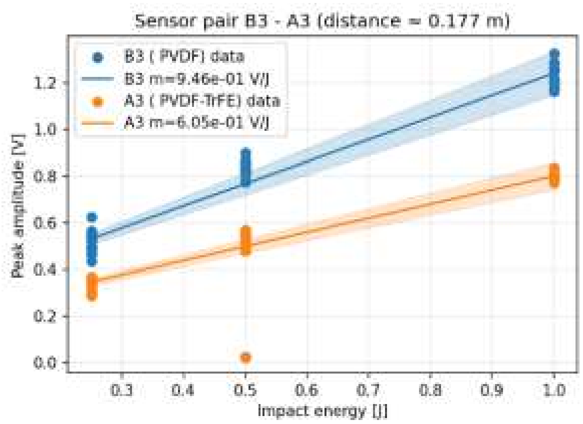

Figure 20. Sensitivity for PVDF-based sensors at 177 mm from the point of impact and 90º orientation.

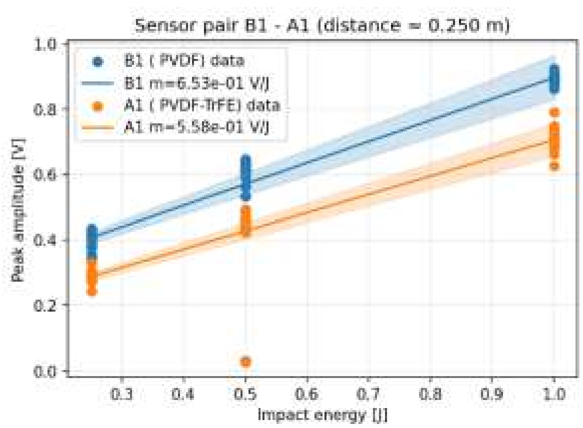

Figure 21. Sensitivity for PVDF-based sensors at 250 mm from the point of impact and -45º orientation.

The results for PVDF-based transducers are grouped by distance and are presented in Figure 19 to Figure 21. For each sensor, these figures include the mean sensitivity curve, 95% confidence intervals, and the slope of a linear regression fitted to the amplitude-versus-energy data.

Analysis of the results shown in previous figures indicates that sensor sensitivity depends on the distance between the impact location and the sensor, due to CFRP wave attenuation and wave-front dispersion, and the sensor orientation with respect to the material axes, due to laminate orthotropy.

For both PVDF and PVDF-TrFE sensors, the highest sensitivity is obtained for sensors oriented at 90°, despite the fact that this orientation corresponds to a larger distance from the impact point than other sensor positions. Under purely geometric considerations, the highest sensitivity would be expected at the minimum distance; the observed deviation highlights the influence of material anisotropy.

For ±45° orientations PVDF sensors exhibit the expected behaviour: the further the sensor is placed from the impact point, the lower the sensitivity. PVDF-TrFE sensors show, within the observed dispersion, similar sensitivity at both distances tested, indicating a weaker distance dependence in this configuration. In all analysed cases, the absolute sensitivity of PVDF sensors is higher than that of PVDF-TrFE sensors.

To remove the influence of distance and orientation, a normalized sensitivity indicator was derived for each sensor. Averaging this normalized sensitivity by sensor technology leads to the results presented in Figure 22. In normalized terms, both PVDF-based technologies exhibit comparable sensitivity, although PVDF sensors show lower dispersion across measurements.

Overall, the PVDF and PVDF-TrFE AE sensors have been characterized in terms of sensitivity as a function of distance to the impact point, sensor orientation with respect to the CFRP orthotropic axes, and impact energy level. This characterization constitutes the first step towards developing a quantitative model for estimating impact energy on CFRP plates.

Based on the experimental characterization, the following conclusions can be drawn:

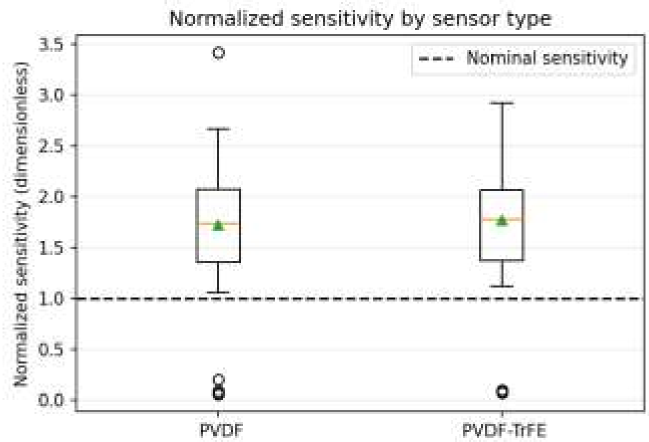

Figure 22. Normalized sensitivity per sensing technology

- Sensor sensitivity is significantly influenced by both the distance to the impact point and the sensor orientation, due to attenuation, wave dispersion and laminate orthotropy.
- In absolute terms, PVDF sensors show higher sensitivity than PVDF-TrFE for all analyzed configurations.
- After normalization to decouple distance and orientation effects, both technologies exhibit similar normalized sensitivity; however, PVDF sensors present lower dispersion.
- The characterized sensitivities provide the basis for developing an impact energy estimation model for CFRP plates. To make this model robust, distance- and orientation-dependent corrections are required.

As a next step, an attenuation model should be developed to correct the sensor response as a function of propagation distance and direction. This model should be integrated into the impact energy estimation pipeline to compensate for the spatial variability in sensitivity and enable more accurate reconstruction of impact energy from AE measurements. Considering the tested characteristics of the selected PVDF-TrFE sensor and the DAQ system specifications, and assuming a reasonable threshold above background noise, the following operating range is defined:

- Minimum acceptable output voltage: ±0.1 V,
- Maximum acceptable output voltage: ±15 V.

Within this range, the sensors are suitable for impacts approximately between 0.2 J and 30 J. For energy levels exceeding this range, signal conditioning will be required to avoid saturation of the acquisition system. In such cases, additional attenuation with a known gain factor must be introduced in the signal chain to preserve linearity and enable quantitative impact energy estimation.

4.3 Sensitivity to temperature

The deployment of PVDF-based acoustic emission sensors in real-world structural health monitoring systems requires reliable operation across broad temperature ranges, from sub-zero conditions to elevated temperatures commonly encountered in outdoor environments exposed to freezing or solar heating. The piezoelectric response of PVDF is inherently temperature-dependent: sensitivity typically varies by approximately 2% per °C over moderate ranges, exhibiting non-linear behavior at the extremes and decreasing sharply near the Curie transition (~130–150°C).

Failure to characterize sensor sensitivity across the intended operating envelope may result in substantial errors in impact-energy estimation, missed detections due to reduced amplitude, or inaccurate localization when amplitude-based thresholding is used. To address these risks, the standard room-temperature impact-sensitivity procedure is extended here to include systematic characterization at both low and high temperatures. This enables the derivation of temperature-compensated calibration factors and supports robust deployment of PVDF-TrFE sensors in thermally variable environments.

The methodology adopted for temperature-dependent sensitivity characterization is described below. The specimen is first conditioned to the selected target temperature inside a programmable thermal chamber, remaining there long enough to ensure thermal equilibrium. Because impact testing must be conducted at room conditions (20°C and 50% relative humidity) and cannot be executed inside the thermal chamber, a small deviation from the target temperature is expected. Consequently, this analysis should be interpreted as qualitative rather than strictly quantitative.

Once the target temperature is reached, the specimen is removed from the thermal chamber, the sensor wiring harness is connected, and the room-temperature drop-weight procedure is repeated for each stabilized temperature at the plate's center for the 1J energy level. A thermocouple attached to the specimen surface using Kapton film is used to record the actual surface temperature (see Figure 23). Temperature monitoring during the test is performed using a QuantumX MX840B universal data-acquisition module.

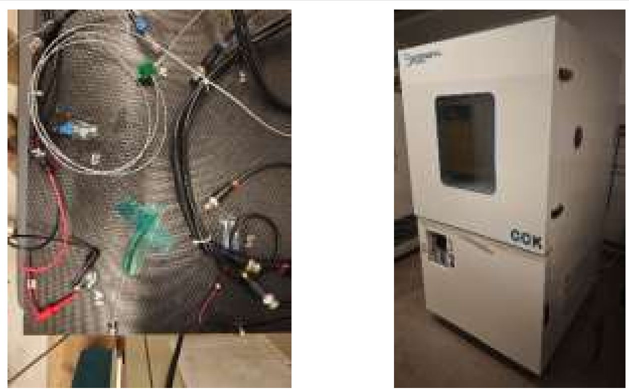

Figure 23. Detail of the temperature sensor placement on the CFRP plate surface (left) and climatic chamber used in the tests (right).

The specimen is conditioned for up to two hours inside a Dycometal CCK programmable thermal chamber (Figure 23) to ensure temperature stabilization. Four conditioning temperatures are considered: –30°C, –10°C, 50°C, and 70°C. Due to the low thermal inertia of the specimen, rapid temperature changes are observed during the first minute after removal from the chamber, followed by an approximately linear temperature evolution throughout the remainder of the test, as illustrated in Figure 24.

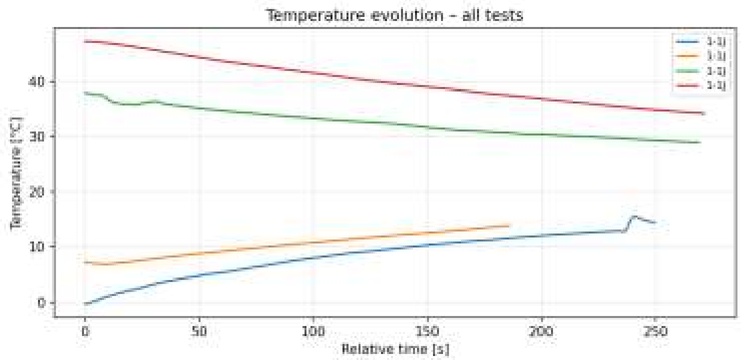

Figure 24 Specimen's temperature evolution during the impact tests.

The exact synchronization between the temperature measurements and the impact events will be established in subsequent phases of the project. This synchronization will enable the development of a temperature-compensation procedure to be integrated into the impact-energy estimation algorithm.

For the purposes of the present qualitative assessment, the experimental results are grouped according to reference temperature labels of 0, 10, 20, 30 and 40, which correspond respectively to tempering conditions of −30°C, −10°C, room temperature (20°C, 50% RH), 50°C and 70°C. These labels are used solely for presentation and comparison and do not yet reflect the precise synchronization between temperature and each individual impact.

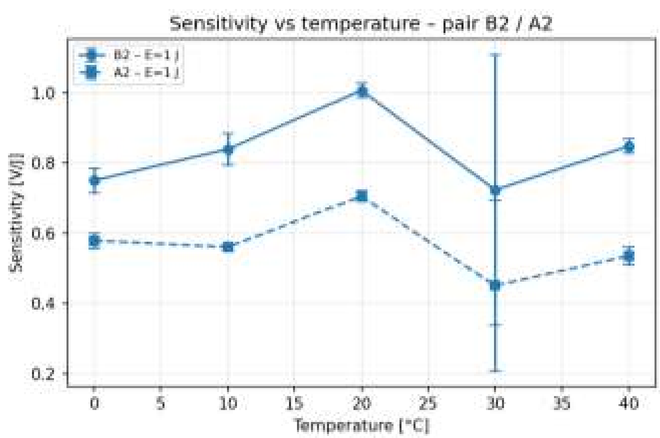

Figure 25. Sensitivity variation as function of temperature for PVDF-TrFE (A2) and PVDF (B2) sensors. 1J impact, 150 mm from the point of impact and +45º orientation.

Figure 25 to Figure 27 show the variation of sensor sensitivity with temperature for the three analysed distances and for both PVDF-based AE transducer technologies. The results include all repetitions without any form of data curation, in order to preserve and display the intrinsic variability of the measurements. It is noted that the dispersion bands for the tests performed at 30°C are significantly wider than those for the other temperature conditions. This behaviour is traced to an atypical result observed during the corresponding test series. As no outlier removal procedure has been applied, these deviations remain visible in the sensitivity distributions, providing a transparent representation of the experimental variability.

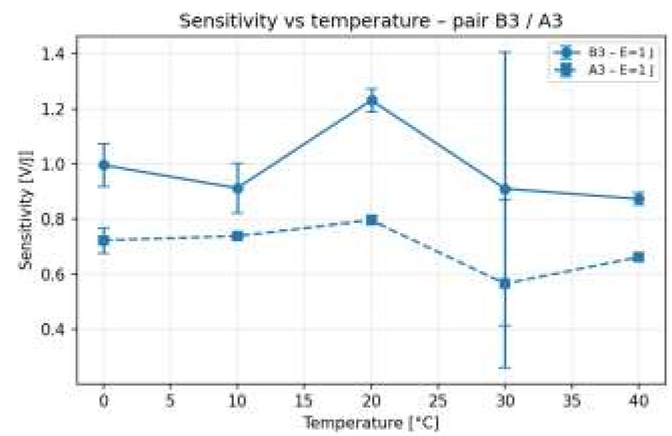

Figure 26. Sensitivity variation as function of temperature for PVDF-TrFE (A3) and PVDF (B3) sensors. 1J impact, 177 mm

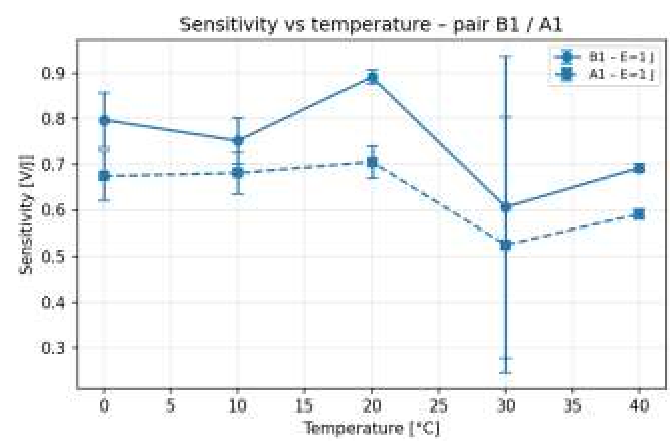

Figure 27. Sensitivity variation as function of temperature for PVDF-TrFE (A1) and PVDF (B1) sensors. 1J impact, 250 mm from the point of impact and -45º orientation.

The highest sensitivity for both PVDF-based sensor technologies is observed at room temperature for all analysed distances. When the temperature is reduced, the sensor sensitivity decreases accordingly, with a more pronounced trend for sensors located closer to the impact point.

A reduction of sensitivity is also observed when the temperature increases. Excluding the measurements corresponding to the 30°C conditioning level, which exhibit atypical behaviour and increased dispersion, the lowest sensitivities are consistently obtained at high temperature across all distances and for both sensing technologies. The only exception is the PVDF sensor placed at 150 mm, for which the trend is noticeably weaker.

Since the variation of sensitivity with temperature is clearly observable—reaching deviations of up to 20% for the PVDF-TrFE sensor oriented at 90°—an extensive experimental campaign is recommended. This expanded test plan should allow incorporating the temperature dependence of sensitivity into the impact-energy estimation methodology that will be developed in subsequent stages of the project.

5. CONCLUSIONS

This deliverable has established a comprehensive basis for the selection, integration, and sensitivity evaluation of a hybrid sensor network for structural health monitoring (SHM) of composite aerostructures, combining magnetostrictive ribbons and piezoelectric sensors as described in the DoA according to the objectives of the project. The work addresses both strain-based damage detection in critical areas and acoustic emission–based impact monitoring, aligned with the operational requirements of composite structures in service.

Magnetostrictive CoSiB flat ribbons (20 µm thickness) were selected for strain monitoring due to their wide sensing range, flexibility, and compatibility with inductive interrogation techniques, enabling localized measurements without complex wiring networks. In parallel, PVDF-TrFE piezoelectric film sensors (Ø6 mm, 40 µm thickness) were selected for impact detection, balancing sensitivity, thermal stability, cost, and manufacturability constraints.

The AFP-based integration concept has been experimentally validated at a proof-of-concept level. Both magnetostrictive ribbons and PVDF-TrFE sensors demonstrated mechanical compatibility with automated fibre placement, confirming that sensor-embedded tapes can be processed without damage when respecting geometric constraints. This represents a key step towards scalable manufacturing of "smart" composite structures.

Sensitivity analyses confirmed the capability of the proposed sensing technologies to detect relevant damage mechanisms. Magnetostrictive patches successfully identified and localized impact-induced damage with results consistent with ultrasonic inspection, demonstrating their effectiveness for strain-based damage detection. While piezoelectric sensors enabled quantification of impact sensitivity in terms of voltage per unit energy, establishing a measurable relationship between acoustic emission signals and impact energy.

The influence of operational conditions on sensor performance has been clearly identified. For piezoelectric sensors, sensitivity depends strongly on distance, orientation, and laminate anisotropy, while temperature variations can lead to deviations of up to ~20% in sensor response. These findings highlight the need for compensation models to ensure robust SHM performance under realistic conditions.

Despite the promising results, several technical challenges remain. The most critical limitation concerns the reliability of sensor integration, particularly for piezoelectric sensors. Initial trials revealed insufficient bonding between PVDF-TrFE sensors and the vitrimer matrix when relying solely on resin tack, leading to poor strain transfer and non-functional measurements.

For magnetostrictive sensors, although embeddability is favourable, functional validation after integration is still pending. Additionally, embedding during curing introduces measurement offsets due to residual stresses and microstructural changes (annealing effects), which must be quantified and compensated.

More broadly, embedding sensors within composite laminates introduces several systemic challenges:

- reliable electrical connection routing without compromising structural integrity,
- ensuring sensor survivability under thermal and pressure loads during manufacturing,
- maintaining consistent bonding quality and strain transfer, and
- managing process variability (e.g. prepreg surface condition, AFP parameters).

To address these limitations, a structured set of activities has been defined for the next project phases. Integration processes will be refined through optimisation of AFP parameters and the use of improved vitrimer prepreg tapes with higher resin content to enhance bonding quality. In parallel, alternative high-temperature-resistant adhesive interlayers will be evaluated if required.

Sensor design improvements are also planned, including the development of PVDF-TrFE sensors with integrated thin-film wiring to enable reliable electrical connections and functional verification after embedding. Additional integration trials will be conducted to validate these improvements under representative manufacturing conditions.

On the sensing side, further experimental campaigns will focus on:

- quantitative functional validation of embedded sensors,
- development of attenuation and orientation correction models for acoustic emission signals, and
- implementation of temperature compensation strategies for robust impact energy estimation.

These activities will culminate in the development of a calibrated and reliable SHM system capable of operating under realistic aerostructure conditions, with results to be consolidated in subsequent deliverables.

Overall, the work performed in this deliverable demonstrates the feasibility and strong potential of integrating hybrid sensor networks into composite aerostructures using AFP-compatible processes. While key integration and calibration challenges remain, the identified solutions and planned developments provide a clear pathway towards achieving a robust, manufacturable, and scalable SHM solution within the TOSCA framework, in agreement with the objectives of the project.

[redacted]